JGR Solid Earth

RESEARCH ARTICLE
10.1029/2024JB030909

New Insights Into Western Antarctic Peninsula Magmatism From Joint Inversion of UAV Magnetic and Gravity Data

Tom A. Jordan[1], **Maximilian Lowe**[1,2], **and Teal R. Riley**[1]

[1]British Antarctic Survey, Cambridge, UK, [2]Institute of Geosciences, Kiel University, Kiel, Germany

Key Points:

- Gravity, magnetic and photographic data from a Windracers Ultra UAV is used to investigate the Antarctic Peninsula crustal structure
- Joint inversion shows ~20% of the crust is formed of mafic intrusives emplaced c. 50 Ma, imagery shows subsequent trench parallel deformation
- Results reflect progressive shutdown of subduction impacting both crustal magmatism and deformation, likely via changing mantle flow

Supporting Information:

Supporting Information may be found in the online version of this article.

Correspondence to:

T. A. Jordan,
tomj@bas.ac.uk

Citation:

Jordan, T. A., Lowe, M., & Riley, T. R. (2025). New insights into western Antarctic Peninsula magmatism from joint inversion of UAV magnetic and gravity data. *Journal of Geophysical Research: Solid Earth*, *130*, e2024JB030909. https://doi.org/10.1029/2024JB030909

Received 3 DEC 2024
Accepted 7 JUL 2025

Author Contributions:

Conceptualization: Tom A. Jordan, Teal R. Riley
Data curation: Tom A. Jordan, Maximilian Lowe
Investigation: Tom A. Jordan, Maximilian Lowe
Methodology: Tom A. Jordan, Maximilian Lowe
Software: Maximilian Lowe
Visualization: Tom A. Jordan, Maximilian Lowe
Writing – original draft: Tom A. Jordan
Writing – review & editing: Tom A. Jordan, Maximilian Lowe, Teal R. Riley

Abstract The Antarctic Peninsula is a unique sector of the circum-Pacific continental margin arc where subduction ceased due to a series of ridge-trench collisions, preserving a relatively un-deformed magmatic arc. This region, therefore, has the potential to provide key insights into how subduction systems behave during their final stages. However, the remote nature of the region means that both geological and geophysical data coverage is often sparse, limiting the ability to interpret its tectonic evolution. Here we present a new analysis of gravity and magnetic data collected from a Windracers Ultra Uncrewed Aerial Vehicle (UAV). The survey targeted a 75 × 25 km region where the Antarctic Peninsula bends and magnetic signatures change, which has been attributed to the onshore influence of adjacent oceanic transform faults running approximately orthogonal to the Peninsula. Using joint inversion of magnetic and gravity data based on a "Variation of Information" approach, we show the region is dominated by two large intrusions, of likely granodiorite composition. Our data indicate little evidence for structural control on magma emplacement, however, coincident imagery suggests that after magma emplacement the region was subject to significant deformation approximately parallel to the Peninsula margin. We interpret these features in terms of the processes occurring as subduction ceased.

Plain Language Summary The Antarctic Peninsula was formed over millions of years from a string of volcanoes and the underlying pools of magma, which turned to solid rock. The processes which control where and how these magmatic rocks formed are related to subduction, the process where dense oceanic crust is forced under the continental margin, releasing water, and triggering melting. Unfortunately, due to sparse data coverage and harsh working conditions the details of these important processes are poorly understood. Using a Windracers Ultra UAV, adapted for environmental science data collection, we collected high resolution gravity and magnetic measurements over an area where the pattern of magmatism was known to change. Using joint inversion of this data, where a computer model finds the rock properties which simultaneously match gravity and magnetic data, assuming magnetic and density (gravity) properties of the rocks are linked, we reveal the shape and type of the hidden rocks. These shapes and rock properties are interpreted, together with photographs of remote rocky islands, to give insights into the subduction processes occurring on the Antarctic Peninsula 20–50 million years ago.

1. Introduction

The Antarctic Peninsula is a long-lived magmatic arc which developed on the Paleo-Pacific margin of Gondwana. Unusually, subduction ceased in this region without the closure of the adjacent ocean, preserving a unique record of arc magmatism (Larter & Barker, 1991). Of especial interest is the apparent link between oceanic fracture zones and the pattern of deformation and magmatism within the continental margin (Johnson, 1997). Using new high resolution geophysical data, we aim to better understand the magmatic processes occurring in this region.

The oldest exposed basement on the Antarctic Peninsula is Early Ordovician in age (~485 Ma) with subsequent magmatism and deformation continuing through the Paleozoic (Millar et al., 2002; Riley et al., 2012b). The Antarctic Peninsula records multiple episodes of extensive magmatism during the Mesozoic (Figure 1), including widespread silicic magmatism during the Jurassic associated with the breakup of Gondwana (Millar et al., 2001; Riley & Leat, 1999). Subsequent arc magmatism, associated with ongoing eastward subduction of the Phoenix Plate beneath the Antarctic Peninsula, peaked at c. 100 Ma (Leat et al., 2009; Riley et al., 2018; Vaughan et al., 2012). From ~50 Ma subduction began to cease as the Phoenix spreading center arrived at the continental margin. Subduction and associated arc magmatism, stopped from the south to the north, with ridge trench collision outboard from Marguerite Bay occurring at c. 19.9 Ma and adjacent to Adelaide Island at c. 16.7 Ma (Larter & Barker, 1991; Larter et al., 1997). Each ridge-trench collision was distinct due to fracture-zones, which

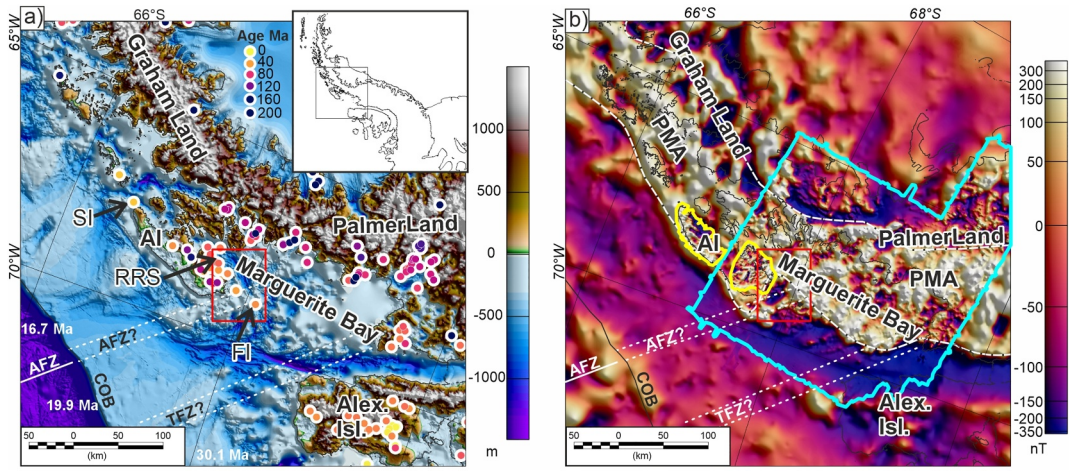

Figure 1. Regional topography and magnetic anomalies of the central Antarctic Peninsula region. (a) Subglacial topography and bathymetry from Bedmachine Antarctica v3 (Morlighem et al., 2020). Inset locates study in Antarctica. Red box locates Figures 2 and 3. Solid white lines mark Adelaide and Tula Fracture Zones (AFZ and TFZ) with zone of interpreted continental influence dashed (Johnson, 1997). Colored dots indicate magmatic ages (Burton-Johnson et al., 2023). White numbers denote age of ridge-trench collision (Larter & Barker, 1991). Abbreviations; Continent Ocean Boundary (COB), Adelaide Island (AI), Alexander Island (Alex. Isl.), Sillard Islands (SI), Rothera Research Station (RRS) and Faure Islands (FI). (b) Regional magnetic data from ADMAP2 (Golynsky et al., 2018), with data from sub-surveys flown in 1990/91 (blue outline) (Johnson & Swain, 1995) and 2010 (yellow outlines) (Jordan et al., 2014). Dashed white lines enclose the composite positive magnetic Pacific Margin Anomaly (PMA) (Johnson, 1999).

segmented both the spreading ridge and subducting plate. Magmatism today, is restricted to the northern tip of the Antarctic Peninsula on the South Shetland Islands crustal block.

Marguerite Bay is an embayment on the western side of the Antarctic Peninsula separating Adelaide Island and Alexander Island (Figure 1a). It is ~130 km wide from N to S and marks a ~90 km inboard step in the coastline. The embayment corresponds with a ~60° change in strike of the Antarctic Peninsula and the transition between the generally narrower and lower elevation Graham Land region to the north and the broader Palmer Land region in the south. Regional aeromagnetic data is marked by the ~3,000 km long positive magnetic Pacific Margin Anomaly (PMA) (Figure 1b) attributed to intrusive rocks emplaced due to the protracted arc magmatism along the Antarctic Peninsula (Johnson, 1999). In detail, the PMA also shows changes across the Marguerite Bay area (Figure 1b). Over northern and western parts of Adelaide Island narrow linear anomalies with a NNE trend reflect the last stages of magmatism within this part of the Antarctic Peninsula (Jordan et al., 2014). These linear anomalies stop on the edge of Marguerite Bay, while the main band of PMA magnetic anomalies continues inboard. Within Marguerite Bay the main magnetic anomalies appear to form a series of offset blocks bounded by major fault zones attributed to linking of oceanic fracture zones to continental deformation during regional magmatism and extension (Johnson, 1997).

Inboard of Marguerite Bay the intrusive rocks associated with the PMA are predominantly dated to c. 100 Ma. In contrast intrusive rocks on the eastern part of Adelaide Island and on Alexander Island are dated to between 44 and 58 Ma (Figure 1a) (Burton-Johnson et al., 2023; McCarron & Millar, 1997; Millar et al., 2001; Riley et al., 2012a). On the Faure Islands within Marguerite Bay, massive intrusive tonalite, quartz-diorite, and gabbro, indicating a hybrid magma source, are dated to 48–47 Ma (Karaoğlan et al., 2023), reflecting some of the last stages of magmatism in Marguerite Bay. Further north, on the Sillard Islands (Figure 1a), magmatism associated with the linear magnetic anomalies is dated to c. 23 Ma (Jordan et al., 2014). These younger ages are not seen in magmatic rocks in Marguerite Bay, but apatite fission track data points to a rapid cooling/uplift event ~20 Ma on the Faure Islands (Karaoğlan et al., 2023) and elsewhere on the western margin of the Antarctic Peninsula (Twinn et al., 2022). This uplift has been attributed to opening of a local slab window due to the cessation of subduction and may be part of the same tectonic event which drove magmatism on western Adelaide Island (Jordan et al., 2014; Karaoğlan et al., 2023), but the presence of a slab window has been contested (Twinn et al., 2022).

The apparent offset of upper crustal blocks seen in magnetic data from the Marguerite Bay region is attributed to interaction between adjacent oceanic transform faults and the overriding continental margin. However, the detailed structure and composition of the intrusions, and the form and extent of the continental faulting has not been resolved. In this study, we analyze new aeromagnetic and aerogravity data that crosses the proposed onshore continuations of the Adelaide Fracture Zone (Johnson, 1997). The data was collected over the northern part of Marguerite Bay using the first deployment in Antarctica of a long-range Windracers Ultra UAV (Figure S1a in Supporting Information S1) (Jordan et al., 2025). Using joint inversion of airborne gravity and magnetic data based on the "Variation of Information" (VI) approach (Lösing et al., 2023; Lowe, Jordan, Moorkamp, et al., 2024; Moorkamp et al., 2011), we investigate the structure and composition of the intrusions. In addition, we analyze opportunistic GoPro® camera footage collected on the survey flights to provide structural information on the remote Faure Islands.

2. Methods

2.1. Survey Design, Platform and Instruments

To interpret the origin of the tectonic structures observed in Marguerite Bay we carried out a new aerogeophysical survey as part of the wider "SWARM" project demonstrating the capabilities of the Windracers Ultra UAV as a platform for Antarctic environmental science (Jordan et al., 2025). The Windracers Ultra platform is a fixed wing UAV with a wingspan of 10 m, a payload of up to 100 kg and a range of up to 1,000 km. The platform was operated from the crushed rock airstrip at Rothera Research Station. It was directed by a ground-controller and routine missions were flown fully autonomously, including take-off and landing. The survey collected gravity and magnetic data within a 25 × 75 km region (Figure 1a) grid south of Rothera Research Station in February/March 2024. The survey had a line spacing of 2 km and was conducted at an altitude of 500 m above the sea surface, increasing to 800 m altitude on a single line over Jenny Island (Figure S1c in Supporting Information S1). The survey orientation placed the main flight lines orthogonal to the trend of the offsets seen in the previous magnetic data over Marguerite Bay (Johnson, 1997), providing the best opportunity of resolving the detail of these structures.

Airborne gravity data was collected using an iMAR iCORUS Strapdown Airborne Gravity system. This light-weight (∼18 kg) thermally stabilized strapdown gravity sensor was installed at the approximate center of mass of the UAV (Figure S1b in Supporting Information S1). Magnetic data were collected simultaneously with the gravity data using a GEM System's GSMP-35U potassium scalar magnetometer. The magnetometer was mounted in the rear door of the Ultra UAV, with the data logger, fluxgates and IMU fixed to the payload floor (Figure S1b in Supporting Information S1). In addition to gravity and magnetic data downward looking imagery was collected at 1 s (∼30 m) intervals using a GoPro® camera, including an internal GPS based time stamp. The camera was mounted on the UAV floor giving a broad overview of the terrain overflown.

2.2. Data Processing

Gravity anomalies were recovered from the recorded GNSS and INS data using the commercial GNSS processing package TerraPos, with subsequent statistical leveling implemented in the Geosoft™ software package to minimize line to line noise (Jordan, Robinson, et al., 2024; Jordan et al., 2025). After leveling the error of the gravity data, calculated from the standard deviation of the difference between repeat flights, was 1.66 mGal. Line gravity data were interpolated onto a 1 km mesh raster using a minimum curvature algorithm implemented in the Geosoft software package. The initial stage of processing provided gravity disturbances, referenced to the ellipsoid, which were further corrected to free air anomalies referenced to the EIGEN-6C4 geoid (Figure S2a in Supporting Information S1). The free air anomalies are dominated by the signature of the local bathymetry (Figure S2b in Supporting Information S1). We therefore implemented a full Bouguer correction calculated out to a radius of at least 165 km, using topographic, bathymetric and ice thickness data from Bedmachine Antarctica (Morlighem et al., 2020). The topographic data were interpolated onto a 1 km mesh raster and the Bouguer correction calculated at an observational altitude of 500 m, equal to the flight elevation of the majority of the survey. Standard densities of 2,670, 915, and 1,028 $kg{\cdot}m^{-3}$ were assumed for rock, ice and water respectively. Rock and ice above the observation altitude in mountain ranges around the survey area were assumed to generate a negative field, proportional to their density, height and thickness. The correction was calculated using a GLQ prism method (von Frese et al., 1981), with the gravity impact of ice, water and rock below and above the survey

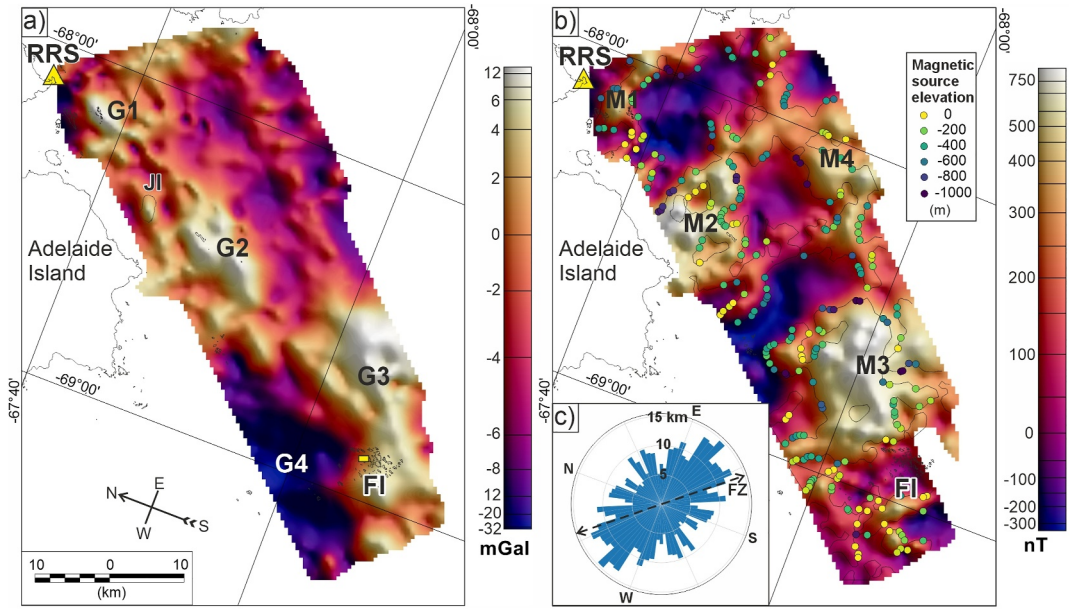

Figure 2. Data sets input into joint inversion. (a) Airy isostatic gravity anomaly. Yellow triangle indicates Rothera Research Station (RRS). Small yellow rectangle locates GoPro image (Figure 5). G1-G4 indicate gravity anomalies discussed in the text. JI: Jenny Island, FI: Faure Islands. For flight lines see Figure S1c in Supporting Information S1. (b) Reduced to pole total field magnetic anomaly. Contour shows 0° tilt angle marking theoretical edge of source bodies and colored dots indicate theoretical source elevation. M1-M4 indicate magnetic anomalies discussed in the text. (c) Rose diagram of source body edge strike, from the direction of 0° tilt angle contour, showing cumulative length in each 5° direction. FZ marks approximate projected direction of Adelaide Fracture Zone (Johnson, 1997).

altitude calculated as separate layers and summed to give the full correction. We note that there is not complete bathymetric coverage of the study area (Dorschel et al., 2022) (Figure S2b in Supporting Information S1), which may introduce artifacts into the recovered Bouguer gravity anomaly. Features away from bathymetric coverage should be interpreted with some caution. However, the presence of numerous small islands indicates relatively shallow water, consistent with the interpolation across the gaps in swath coverage. Additionally, visually, no significant artifacts, such as abrupt jumps in the Bouguer anomaly are apparent (Figure S2c in Supporting Information S1), suggesting the interpolated bathymetry is a reasonable approximation.

A further correction for the gravity effect of varying crustal thickness was made assuming the observed topography/bathymetry was isostatically compensated at the Moho. This correction was calculated using GMT (Wessel et al., 2013), with the routine gravfft assuming a reference Moho depth of 23 km, in line with a continental wide reference model of crustal thickness from gravity data constrained by sparse seismic observations (Pappa et al., 2019). We assumed an Airy isostatic compensation model, with densities for the crust and mantle of 2,670 and 3,300 $kg{\cdot}m^{-3}$ respectively, giving a smooth model of the gravity field due to a theoretical isostatically balanced Moho (Figure S2d in Supporting Information S1). After subtracting the isostatic correction from the Bouguer anomaly, the Airy Isostatic residual gravity anomaly provides the most easily interpretable view of the density structures within the upper crust (Figure 2a). We cannot rule out discrepancies due to incomplete understanding of isostatic compensation in the region. However, such discrepancies are likely to be long wavelength in nature and have minimal impact on the bodies recovered by our joint inversion.

The new magnetic data were subject to standard corrections for aircraft motion, diurnal variations, and the International Geomagnetic Reference Field (IGRF) (Jordan, Lowe, et al., 2024; Jordan et al., 2025). In addition, the line data were leveled to match existing higher altitude airborne surveys, with between 1.5 and 3 km line spacing, provided via the ADMAP2 compilation (Golynsky et al., 2018; Johnson & Swain, 1995). The statistical leveling procedure was carried out after all data was upward continued to 2,440 m, the highest elevation for the data in this region from ADMAP2. The calculated leveling correction was then applied to the new UAV data-set at the 500 m observation altitude, allowing the resolution of the more recent lower altitude data to be maintained (Jordan, Lowe, et al., 2024; Jordan et al., 2025). To minimize the distortion of the shape and position of the magnetic

anomalies relative to their sources the gridded magnetic data was reduced to the pole (RTP) (Cooper & Cowan, 2006), using local values of inclination and declination from the IGRF model of −59.59° and 20.07° respectively (Figure 2b). Low magnetic latitudes, the presence of significant remnant magnetization, or complex anomaly patterns can lead the RTP procedure to introduce significant artifacts into the field. These conditions do not appear to be relevant in our study area and artifacts associated with the transformation are therefore likely to be minor.

To highlight the edges of magnetic source bodies, and to make a first approximation of their depth, we applied the tilt angle digital enhancement (Salem et al., 2007). This places the 0° tilt angle contour over the source edge, while the distance to the adjacent positive and negative tilt contours gives an approximation of source depth, assuming no remanence and vertical contacts (Figure 2b). We used the distance to the ±30° contours to calculate depth, rather than the standard 45° contours (Salem et al., 2007), as they are closer to the zero contour, hence are less disturbed by interference between adjacent anomalies. Deviations between the depths recovered from and the directions to the positive and negative 30° tilt contours were used to screen for the reliability of the recovered depths (Jordan & Becker, 2018). To estimate the dominant trends in the magnetic data we used the direction and length between each node of the 0° tilt angle contour. The cumulative length in each 5° directional bin from 0 to 180° was calculated and plotted on a rose diagram to highlight any trends (Figure 2c). For display the data was reflected to create a full 360° image.

2.3. Inversion Scheme

Recovering lithology, source geometry or volume from gravity or magnetic data alone is challenging as models of such potential field data are non-unique. Forward models as presented in the literature, although mathematically robust, are often subjective, as researchers directly define source geometry, density and susceptibility, using their knowledge and assumptions about a region. This can give a good fit to the data, but subjective assumptions are embedded in the model result. In contrast inversions reduce the subjective influence of the researcher and enhance reproducibility, yet they can struggle to provide geologically plausible results. Specifically working with gravity and magnetic data independently in inversion schemes often fails to resolve the base or deeper edges of bodies due to the non-unique nature of the solutions.

One method to help overcome the limitations of independent inversion of gravity or magnetic data is to use a joint inversion approach. Gravity and magnetic anomalies are typically generated within the crust by bodies with set geometries and relatively consistent internal density/susceptibility ratios, which contrast with the density/susceptibility of their surroundings. This means that the geometry which generates the magnetic anomaly must also create the gravity anomaly and vice versa. By considering both magnetic and gravity data together the degree of freedom of the inversion is reduced, resulting in a more constrained and geologically plausible result. One method to implement such a joint inversion is to calculate how well the geometry of the susceptibility model predicts the geometry of the density model, and vice versa. This variation of information (VI) parameter can be minimized within an inversion scheme, together with the fit to input gravity and magnetic data allowing constraint of an inversion output beyond what is possible for either a magnetic or gravity inversion alone (Lowe, Jordan, Moorkamp, et al., 2024). This method will work best in areas where the sub-surface bodies have an internally fixed density and susceptibility ratio, which contrasts with the surrounding region. Areas with spatially coincident gravity and magnetic anomalies are likely to fulfill this criteria. Areas with no spatial correlation between gravity and magnetic anomalies may, for example, result in geometric features in the density model associated with the magnetic anomalies. However, the amplitude of these features will be low, reflecting the requirement for the geometry to create a minimal gravity anomaly. We implemented the joint inversion scheme, including VI, using the jif3d joint inversion framework software (Moorkamp, 2021; Moorkamp et al., 2011). The suitability of VI inversion for recovery of subsurface body geometry and properties from gravity and magnetic data has been recently demonstrated in an Antarctic context (Lösing et al., 2023; Lowe, Jordan, Moorkamp, et al., 2024).

Our input data were the Airy gravity and RTP magnetic anomalies, each interpolated onto a 500 m cell size raster. Grids were used as they allowed full and consistent consideration of the field geometry both along and between the flight lines. The inversion data were re-projected from standard polar stereographic, to a projection with a longitude of origin of 45°E, facilitated by use of RTP data which assumes vertical inclination, meaning the inversion in insensitive to rotation of the data. This re-projection enabled us to construct the required rectangular inversion mesh aligned with the survey, minimizing the number of padding cells required to complete the

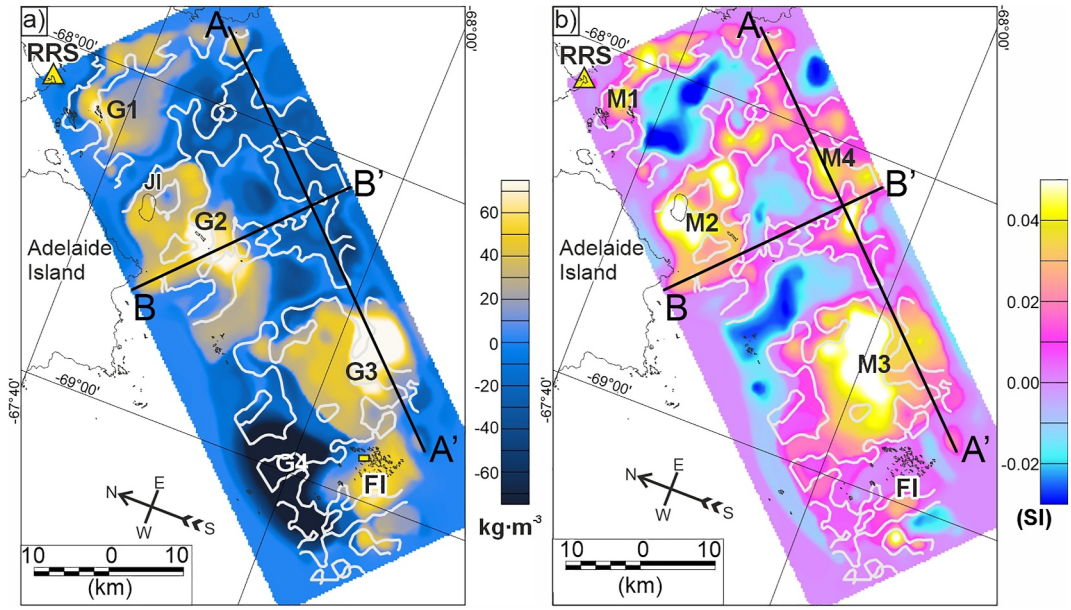

Figure 3. Depth-slices from recovered density (a) and susceptibility (b) data cubes at a depth of 1.9 km. While line locates tilt 0° contour marking theoretical edges of magnetic source bodies. Black lines labeled A-A′ and B-B′ locate profiles in Figure 4.

rectangular mesh, saving significant computational time. Use of RTP data may introduce processing artifacts influencing the inversion result, but the scale of such errors in our study region is likely small and will create minimal bias in our final interpretation.

We assume the base of the model is at 20 km, close to previously estimated Moho depth in this region (Pappa et al., 2019). The inversion space has a vertical cell resolution of 100 m at the top of the model, increasing by a factor of 1.1 with depth, so that cells at 20 km depth have a height of 2,111 m. The model has a constant horizontal resolution of 250 m and an observation altitude of 500 m, coincident with the survey altitude. Bathymetry and topography were from BedMachine Antarctica (Morlighem et al., 2020). The model space was initialized with uniform values of zero for magnetic susceptibility and density. Cells which fell within the water column were fixed so density and magnetic susceptibility could not vary. The imposed error assumption for gravity and magnetic data was 2 mGal and 10 nT respectively. This represents a conservative estimate of the gravity error, estimated to be 1.66 mGal from repeat measurements. The magnetic error is below the 37 nT estimated from internal crossovers of the SWARM magnetic data. However, as the magnetic data were fit by the inversion with error values significantly below this, the inversion scheme is not highly sensitive to this value. We tested a range of coupling factors, which defines how closely the density and susceptibility output must correlate. A value of 20,000 for the final model was chosen as it gave an inversion which converged (Figure S3a in Supporting Information S1) and had low residual errors (Figures S3c and S3d in Supporting Information S1). The inversion was run for 30 iterations which gave an adequate convergence between observed and modeled fields (Figures S3 and S4 in Supporting Information S1). The variation of information was still evolving at this point (Figure S2b in Supporting Information S1), however, further iteration did not improve the fit to the data or model output (see results). The inversion output is a 3D data cube with relative density and susceptibility at each node. This output data set can be sliced horizontally (Figure 3) or vertically (Figure 4), and the association between recovered density and susceptibility can be plotted to aid interpretation of the geological structures and lithology.

2.4. GoPro Feature Analysis

The majority of the survey flights were over open water, however, some crossed remote islands, where basic optical imagery of the exposed rocks can provide additional insights into the regions tectonic structure. Images of the Faure Islands (Figure 2a) were assessed and an image of a representative island, ~600 m long and with limited snow cover, was identified for further analysis (Figure 5). To quantify the structures on the island the image was

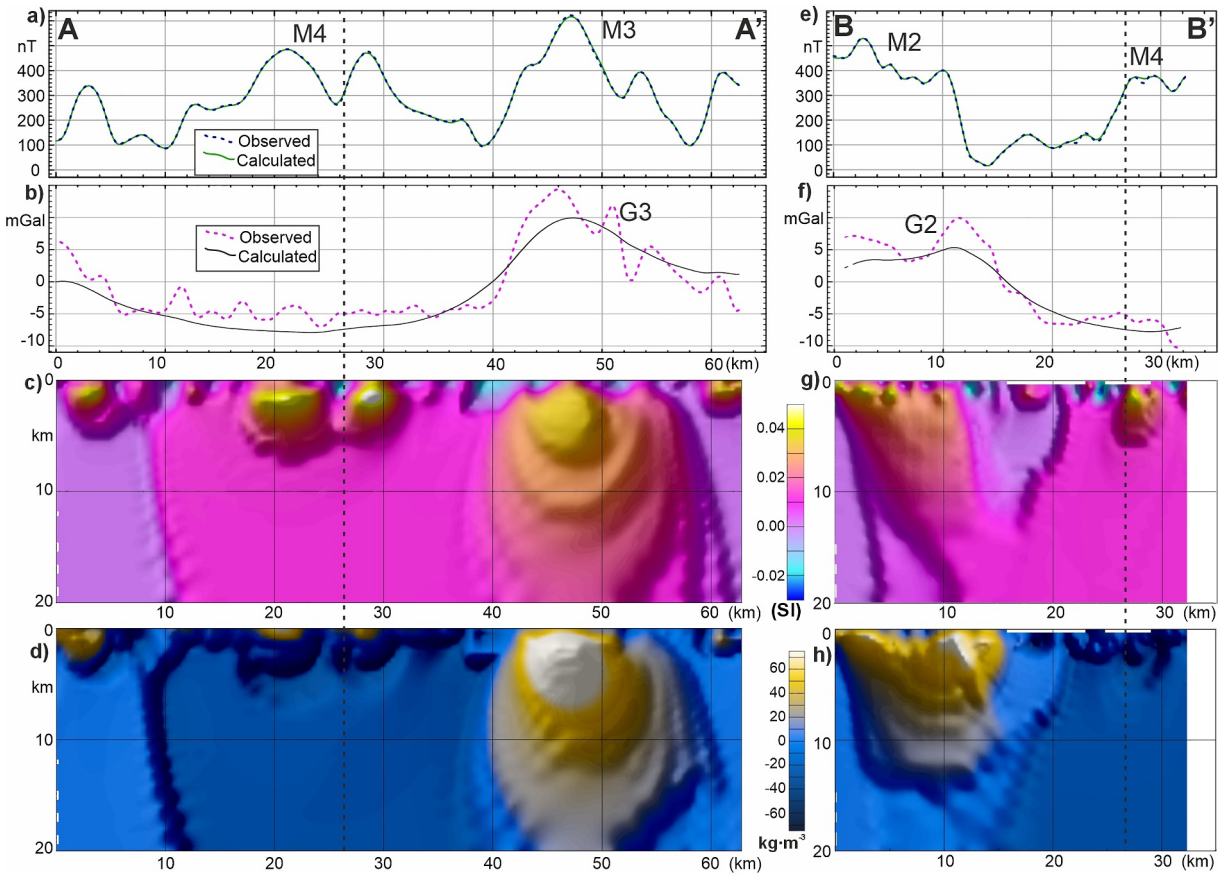

Figure 4. Profiles of inversion input/output and vertical sections of recovered crustal properties. See Figure 3 for location. Vertical dashed line locates intersection. For Profile A panels are: (a) Input and modeled magnetic field. (b) Input and modeled gravity field. (c) crustal susceptibility. (d) Relative crustal density. For Profile B panels are: (e) Input and modeled magnetic field. (f) Input and modeled gravity field. (g) Crustal susceptibility. (h) Relative crustal density.

ortho-rectified based on the image time stamp and UAV position and heading from processed navigation data. Due to poor knowledge of the lens system, it was not possible to precisely adjust the image, however, alignment with independent coast-line information confirm the broad-scale adjustment of the image is correct (Figure 5a). Lineations within the image were identified using the Canny Edge Detection algorithm (Canny, 1986) implemented within the OpenCV python package. Detected edges were extracted as vector objects by contouring the edge raster. Short contours with less than 60 nodes were excluded as likely noise. As we aim to detect linear features, each remaining contour (excluding those in the sea) was fit with a linear trend using the polyfit function from the python numpy library. The length and angle of the extracted linear segments was then used to create a rose diagram indicative of the regional structural fabric on the island (Figure 5c). This automated pick of lineations includes in several cases the edges of snow bodies and sections of the coast. Although not strictly direct images of geological features, we argue that at this scale they most likely reflect topographic features associated with the geology, such as snow filled elongate gullies, or edges of the elongate topographic highs which form the islands themselves.

3. Results

3.1. Gravity and Magnetic Information

The Airy isostatic gravity field across the study region has a mean value of ~0 mGal and shows three broad positive anomalies (G1 to G3) with peak amplitudes of 10–15 mGal (Figure 2a). In addition, in the grid southwest, there is a strong negative anomaly (G4) with an amplitude of <−30 mGal. The magnetic data show similar areas of broad high amplitude anomalies (M1 to M4) with peak amplitudes of 500–1,200 nT (Figure 2b). Anomalies M1-M3 loosely correlate with gravity anomalies G1-G3, but anomaly M4 is associated with indistinct but

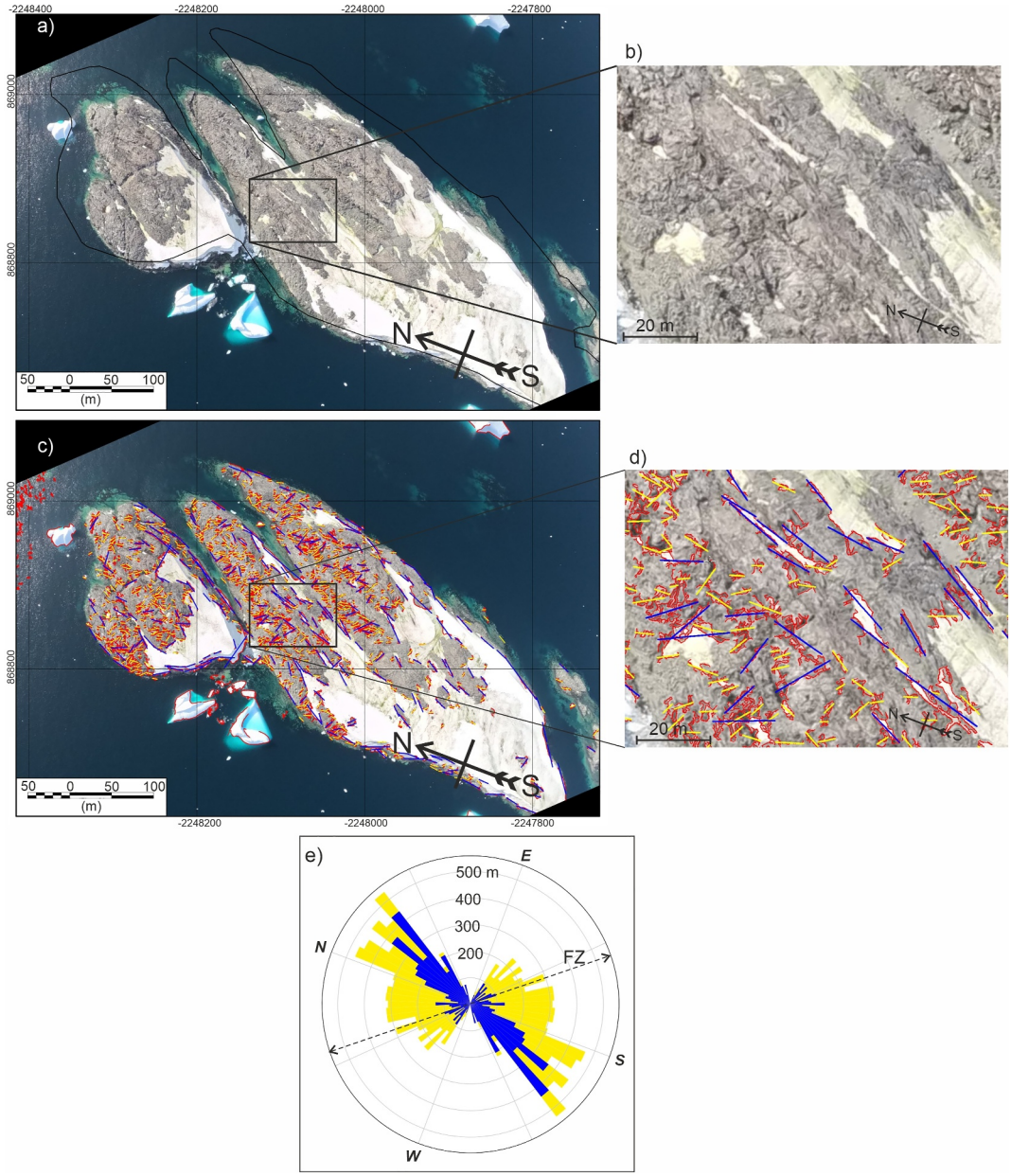

Figure 5. Selected Faure Islands GoPro camera image and analysis. (a) GoPro image after rotation and scaling, note fit to coastline from Antarctic Digital Database (black line). (b) Detail of island at maximum zoom. Note broad NNE trend. (c) Rotated image overlain with edge features from Canny edge detection (red), all best fit linear trends (yellow), and linear features >10 m long (blue). (d) Detail of island with lineations overlain. Note that the automatically picked lineations broadly correspond to the main visually observed trend, although not all apparent lineations are automatically picked. (e) Rose diagram showing total lineation length within five-degree bins. Dashed line (FZ) indicates direction of onshore extension of Adelaide Fracture Zone (Johnson, 1997).

generally negative residual gravity anomalies. Although the magnetic data is marked by long wavelength (10–20 km) positive and negative anomalies, there are also higher frequency anomalies indicative of more complex structure at shallow depths not resolved by the gravity data.

The tilt depth contours outline magnetic anomalies M1-M4, providing a first estimate of the location of key sources. Complexity in the contour pattern, especially associated with M2 and M4 are indicative of multiple overlapping sources, or a geometrically complex source, which together give rise to the observed anomalies. The estimates of source elevations are between −200 and −1,000 m, which indicates the sources are likely at or near

the seabed. This is consistent with geological observations which show igneous rocks of the Adelaide Island Intrusive Suite composed of granodiorite - gabbro hybrid plutons, which are the likely source bodies, exposed on Jenny Island and close to Rothera Research Station (Riley et al., 2011) as well as on the Faure Islands (Karaoğlan et al., 2023). The magnetic source edges show a generally preferred WNW/ESE trend (Figure 2c), however, this preferred direction is not particularly dominant, or well-focused.

3.2. Inversion Results

The inversion returns a model with a range of susceptibility and density values between −0.04 and 0.08 SI and −150 and 100 kg·m^{-3} respectively (Figures 3 and 4). The distribution of recovered density and susceptibility values seem reasonable, with high density and susceptibility values associated with the key positive gravity (G1-G3) and magnetic anomalies (M1-M4) (Figure 3) respectively, as expected. The calculated magnetic anomalies fit the input data well, with a standard deviation of ∼3 nT (Figure S4f in Supporting Information S1, Figures 4a and 4e). The calculated gravity anomalies fit the observed data with an equivalent standard deviation (∼2.5 mGal), however, due to the lower absolute amplitude of the gravity anomalies, the peak amplitudes do not appear as well modeled (Figure S4c in Supporting Information S1, Figures 4b and 4f). The apparent poor fit of the inversion to the observed gravity data reflects a combination of the imposed error threshold of 2 mGal and the imposed coupling between the susceptibility and density values in the model which together prevent a better fit being achieved. Tests show that reducing the gravity error threshold can force the inversion to match the gravity observations better (Figure S5a vs. Figure S5b in Supporting Information S1). However, the improved fit included matching low amplitude (<2 mGal) short wavelength gravity anomalies which may be noise, and gives rise to numerous small and shallow bodies with extreme fluctuations in density, which we are not confident are real. Running the inversion for additional iterations also did not reduce the errors, but rather more sharply defined the breaks in density/susceptibility at the edges of inverted bodies (Figure S5c in Supporting Information S1). The location of such sharply defined edges and specific uniform values of density/susceptibility within bodies are unlikely to be robust, reflecting instead an inversion artifact. We therefore prefer to halt the inversion when the gravity and magnetic error have ceased to converge at ∼30 iterations.

Vertical sections through the inversion result indicate the sources for M2/G2 and M3/G3 are large high susceptibility and dense bodies extending to depths of 10 km or more (Figure 4). In contrast the source for anomaly M4 appears not to exceed 5 km depth. It is apparent from the cross sections that the recovered density and susceptibility models share common structures (Figure 4). A cross plot of the recovered susceptibility and density values (Figure 6a), confirms that the recovered values for physical properties generally lie within distinct clusters. The primary cluster is around a susceptibility and density of zero, the inversion input value. The second most common cluster is for susceptibility and densityof 0.01 (SI) and −25 kg·m^{-3}. When the spatial location of cells forming these two clusters are plotted no clear formation into localized discrete bodies is seen (Figure S6 in Supporting Information S1). We therefore consider that these two clusters reflect the numerical and crustal background values within our study area. By excluding these background values, and only considering values within the other key clusters outlined in colored polygons in Figure 6a, we can create a 3D sub-surface model of the inversion result (Figure 6b and Figure S10 in Supporting Information S1).

A high density (>20 kg·m^{-3}) and susceptibility (>0.0175 (SI)) cluster is noted (Figure 6a, Figures S7 and S10 in Supporting Information S1). This cluster can be split into sub-provinces, reflecting different branches in the cross plot within this broader group (Figure 6a). Spatially this cluster is localized in two main areas associated with positive magnetic and gravity anomalies M2/3 and G2/3, with some association with anomalies M1/G1. The lowest susceptibility/density part of this cluster (Figure S7a in Supporting Information S1) covers the largest area, forming the outer "shell" of the two main recovered bodies. Higher susceptibility/density parts of the wider cluster (Figures S7b–S7d in Supporting Information S1) lie within the main bodies, with the most extreme density and susceptibility clusters localized in different areas. The Supplementary Movie S1 File shows how the constituent parts of the broader high density/susceptibility bodies fit together. The 3D view of the recovered locations with these density/susceptibility relationships shows the two main bodies extending to a depth of ∼20 km with an approximately spherical shape, tapering slightly with depth (Figure 6b, Figure S10 in Supporting Information S1), in line with what is expected from the cross sections of recovered density and susceptibility (Figure 4). A shallower body with the same density/susceptibility relationship is noted in the northern corner of the region associated with anomalies G1/M1 (Figure 6b).

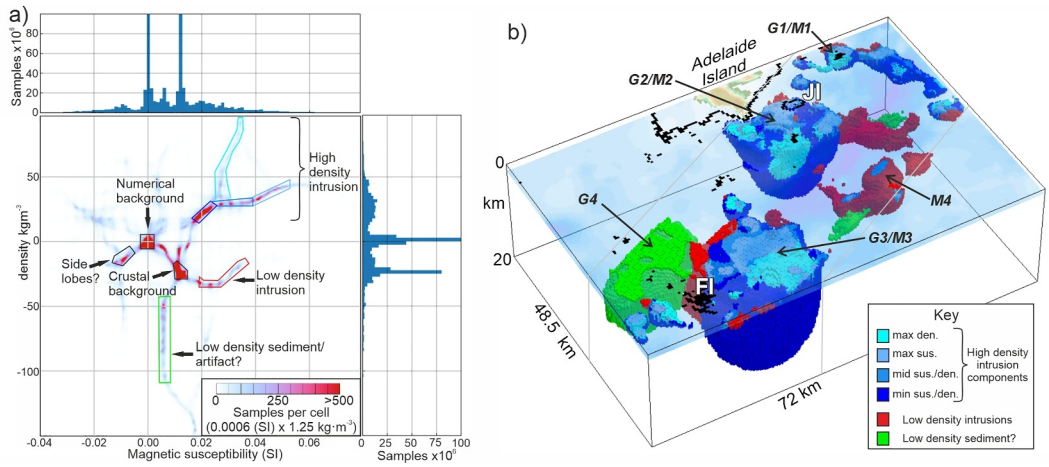

Figure 6. Analysis of density/susceptibility relationship recovered from joint inversion. (a) Cross plot showing density and susceptibility relationship as a heat map. Colored polygons outline main visually significant clusters of density and susceptibility. The 3D spatial location of each of these groupings is shown in panel (b), color coded to match the polygons in panel (a). Black polygons mark clusters of values interpreted to be background values, or potential inversion artifacts. Histograms clipped to 100,000 counts. (b) 3D view of interpreted bodies, looking approximately north. Bodies formed of cells colored according to clusters outlined in panel (a). Black lines mark the coast, with surface elevation as a semi-transparent layer for reference. JI and FI are Jenny Island and Faure Islands respectively. G1-G4 and M1-M4 locate key gravity and magnetic anomalies from previous figures. Gray lines mark approximate edge of study area. See Supporting Information S1 for alternative perspectives (Figure S10 in Supporting Information S1) and for 3D video.

A cluster with negative density and high susceptibility is also observed (Figure 6a and Figure S8a in Supporting Information S1). Spatially this cluster plots in two distinct regions (Figure S8a in Supporting Information S1). In the grid north this cluster is associated with magnetic anomaly M4, while a secondary spatial grouping of the density/susceptibility cluster is seen adjacent to anomaly M3. Because the northern cluster is a localized body associated directly with an identifiable magnetic anomaly, we consider this a reasonable inversion of the source properties causing anomaly M4. In contrast the southern expression of this density/susceptibility cluster lies away from the peak of anomaly M3 and on the boundary between gravity anomalies G3 and G4 (Figure 6b and Figure S10 in Supporting Information S1). This feature may therefore be an artifact of the inversion, forming at the boundary between two other features.

The final set of density/susceptibility clusters are associated with low density (<-50 kg·m^{-3}) and low <0.01 (SI) or even negative susceptibility. The strongly negative density values and low but positive susceptibility values are focused over negative gravity anomaly G4 (Figure S8b in Supporting Information S1) reflecting a low-density source body in this region. In contrast the negative susceptibility values (Figure S9 in Supporting Information S1) are quite widely dispersed and lie over negative magnetic anomalies. These negative susceptibility features are likely artifacts where the inversion works to fit the negative magnetic anomalies with negative susceptibility, rather than as the side-lobes of other positive anomalies.

3.3. GoPro Features

The imagery over the Faure Islands shows that many of the component islands have an apparent linear internal fabric, as seen on the un-named island shown in Figure 5. This fabric is consistent with the direction of the coastline of many of the islands, which appear to be elongated in a NNE/SSW direction. Analysis of lineations extracted from the image using Canny edge detection method (Figures 5c and 5d) confirm the dominant NNE/SSW trend (Figure 5e). Many shorter lineations appear at a high angle to this main trend, but such features are not dominant, and do not appear to cross-cut the main lineations, suggesting they may be an earlier fabric.

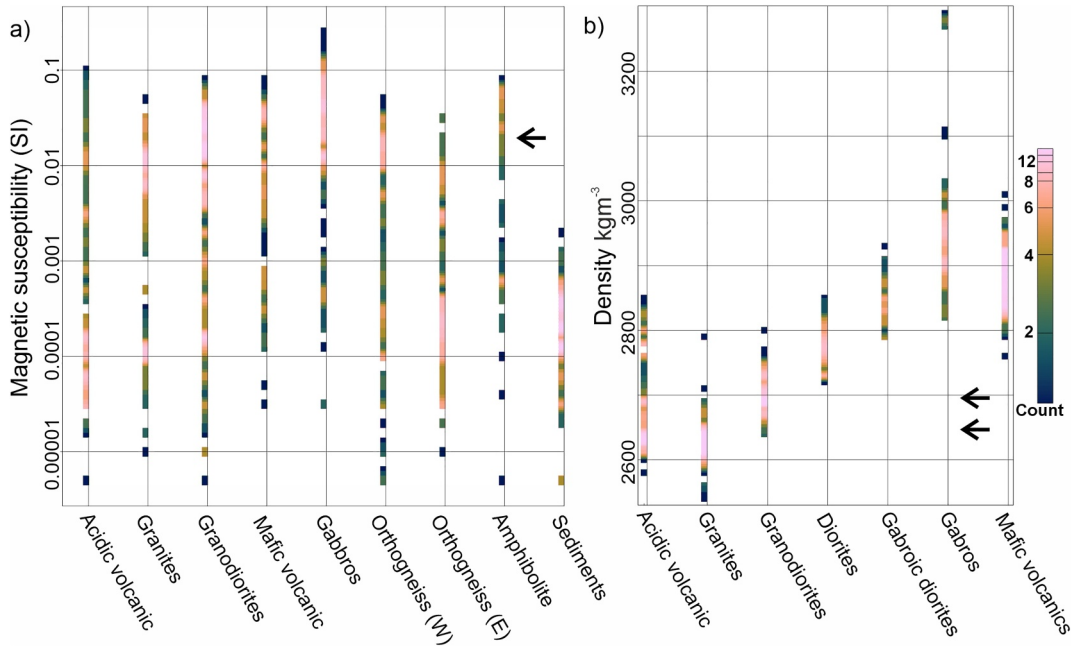

Figure 7. Compilation of Antarctic Peninsula susceptibility and density values. (a) Measured magnetic susceptibility values (Wendt et al., 2013). Black arrow marks approximate value of high susceptibility clusters from joint inversion (Figure 5a). Note Log10 scaling. (b) Density values calculated from the PetroChron Antarctica geochemical database (Sanchez et al., 2021), grouped to approximately the same lithologies as the magnetic values. Arrows show mean of high- and low-density clusters.

4. Interpretation and Discussion

The elevated susceptibility values recovered by our inversion are in line with values measured on igneous rocks across the Antarctic Peninsula (Figure 7a) (Wendt et al., 2013). However, magnetic susceptibility alone is not diagnostic of lithology. Considering the relationship between rock density and susceptibility reduces the ambiguity of inferred rock lithologies interpreted from geophysical inversion (Lowe, Jordan, Ebbing, et al., 2024). The inversion recovers relative density, which can be converted to absolute values based on the reference density used for the Bouguer correction of 2,670 kg·m^{-3}, which is a widely accepted average for crustal rocks. Assuming this conversion, the recovered densities for the key clusters are a little lower than that recovered for many igneous rocks across the Antarctic Peninsula (Figure 7b) (Sanchez et al., 2021), but are in-line with those reported for granites and granodiorites. The distinct higher and lower density clusters we resolve suggest that distinct denser granodiorite bodies form the main features associated with anomalies M1/G1, M2/G2 and M3/G3, while lower density granites form the smaller structures in the east associated with magnetic anomaly M4. The highest recovered densities point toward diorites, or even gabbroic diorites being present in some places. The suggestion that the main bodies are granodiorites is consistent with the observed susceptibility data, which show slightly more positive values than for the granites (Figure 7a), in-line with the longer tail of higher susceptibility values recovered by the inversion for the denser bodies (Figure 6a). Field observations confirm that granodiorites/diorites are a common lithology in the region, outcropping on both Jenny Island and the Faure Islands (Karaoğlan et al., 2023; Riley et al., 2011). However, the main source body for anomalies G3/M3 identified from the geophysical data lies northeast of the Faure Islands (Figure 6b), so may be distinct from the outcrop. Although granodiorites dominate the region, gabbroic rocks are mapped on Jenny Island (Riley et al., 2011), and bi-modal magmatism is suggested on the Faure Islands (Karaoğlan et al., 2023). Hybrid sources within the main magmatic bodies are in-line with the distinct high density and high susceptibility zones identified within the main intrusions, which could reflect bi-modal magmatism. The fact that the inversion does not recover densities high enough to be consistent with the outcropping gabbro may be an artifact of the chosen parameters. If the inversion were tuned to give a better fit to the peak amplitudes observed in the gravity data (Figure 4), higher densities, closer to those expected of gabbro, would likely be recovered.

Gravity anomaly G4 is associated with negative recovered densities, between 2,620 and 2,570 kg·m^{-3}, and low, but non-negative susceptibility values. The associated body extends to a depth of ∼15 km (Figure 6b and Figure S10c in Supporting Information S1). As the bathymetry is not well constrained in this region (Figure S2b in Supporting Information S1), it is hard to be fully confident of this result, due to the uncertainty in the gravity anomaly corrections. However, the presence of several small islands across the region points to shallow water depths, consistent with the interpolated bathymetry grid, so errors in the Bouguer correction are likely to be relatively minor. We suggest two possible interpretations for the body; either a low density and low susceptibility granite, or a relatively low-density sedimentary body. Although low susceptibility granites are present on the Antarctic Peninsula (Figure 7a), studies of measured susceptibility suggest that these rocks are typically focused on the east coast (Wendt et al., 2013). We therefore favor the hypothesis that the recovered body reflects a low-density sedimentary unit. We cannot confidently constrain the thickness of the proposed sedimentary sequence, due to uncertainty about its precise lithology. If the sedimentary body is well lithified material, it may have a density and thickness close to that predicted by the inversion. If the sedimentary unit is less well lithified, it may have a lower density and hence the body would be thinner. As the region is extensively glaciated, soft sediments are likely to have been eroded, and we therefore suggest an older well lithified sedimentary body is more likely to have been preserved. This interpretation is consistent with the geology of the area where Late Mesozoic fore-arc sedimentary rocks outcrop extensively from Alexander Island to the south (Figure 1) and continue northward along the main axis of Adelaide Island. The fore-arc units are predominantly sandstone-shale sequences with rare interbedded volcanic tuffs (Riley et al., 2012a, 2024). Ultimately, direct observations are required to verify this hypothesis.

We interpret the main recovered bodies as intrusive igneous features, associated with arc magmatism, with a most likely age of ∼50 Ma, based on dated exposures on Adelaide Island and the Faure Islands (Karaoğlan et al., 2023; Riley et al., 2012a). It was hypothesized that the apparent segmented nature of the intrusions across Marguerite Bay was due to upper crustal structures created by interaction between the continental crust and the adjacent oceanic fracture zones within the subducting Phoenix Plate (Johnson, 1999). However, our survey, which specifically targeted the proposed structure associated with the continuation of the Adelaide Fracture Zone through the Faure Islands, fails to reveal clear evidence for control of magma emplacement by the fracture zone, either in magnetic or visual data (Figures 2 and 5 respectively). Such evidence would include linear magnetic fabric reflecting magma emplaced along existing or active fault systems, or sharp truncation of bodies which could be attributed to post-emplacement faulting. Instead, the key magnetic anomalies, and associated interpreted magmatic bodies recovered by our inversion, show little evidence of a preferred orientation (Figures 2b and 6b). The trends of the edges of the magnetic anomalies do reveal a slight preference for a WNW/ESE trend, however this is oblique to the expected NE/SW trend of the Adelaide Fracture Zone (Figure 2c). Although we find no clear evidence for deformation of the upper crust associated with the expected fracture zone trend, oceanic fractures split the subducted slab and may therefore influence where magma is generated. The location of the major intrusions, and apparent bands of intrusive rocks observed in magnetic data across Marguerite Bay (Johnson, 1997), may therefore reflect the influence of subducted transform faults on magma generation, rather than faulting in the upper crust.

The relationship between magmatism, deformation and subduction along the Antarctic Peninsula appears to have evolved over time. In Marguerite Bay we find limited evidence of direct structural control on magma emplacement linked to subduction. However, the volume of the two largest interpreted intrusions is ∼7,400 km^3, requiring formation of significant accommodation space and hence an extensional environment in the upper plate around 50 Ma. This interpreted magmatic event coincides with an abrupt slow-down in subduction of the Phoenix Plate between 50 and 40 Ma, and with cessation of subduction between the Tharp and Heezen fracture zones 400–600 km south of Marguerite Bay (Figure 8) (Burton-Johnson et al., 2023; Eagles et al., 2009; Müller et al., 2018). Slowing subduction likely acted to focus slab dehydration (Magni et al., 2014), locally increasing the volume of magma generated. At the same time, opening of a slab window south of Marguerite Bay would have favored toroidal mantle flow around the slab edge driving extension within the over-riding plate and slab role-back (Schellart, 2024). We propose that together these factors created the magma volumes, accommodation space and oceanward shift in the locus of magmatism required to explain the large intrusions we observe in our geophysical interpretation.

Although the main set of intrusive rocks we interpret show relatively limited structural control on emplacement in Marguerite Bay, analysis of the GoPro imagery reveals a well-defined NNE structural fabric (Figure 5e). If this

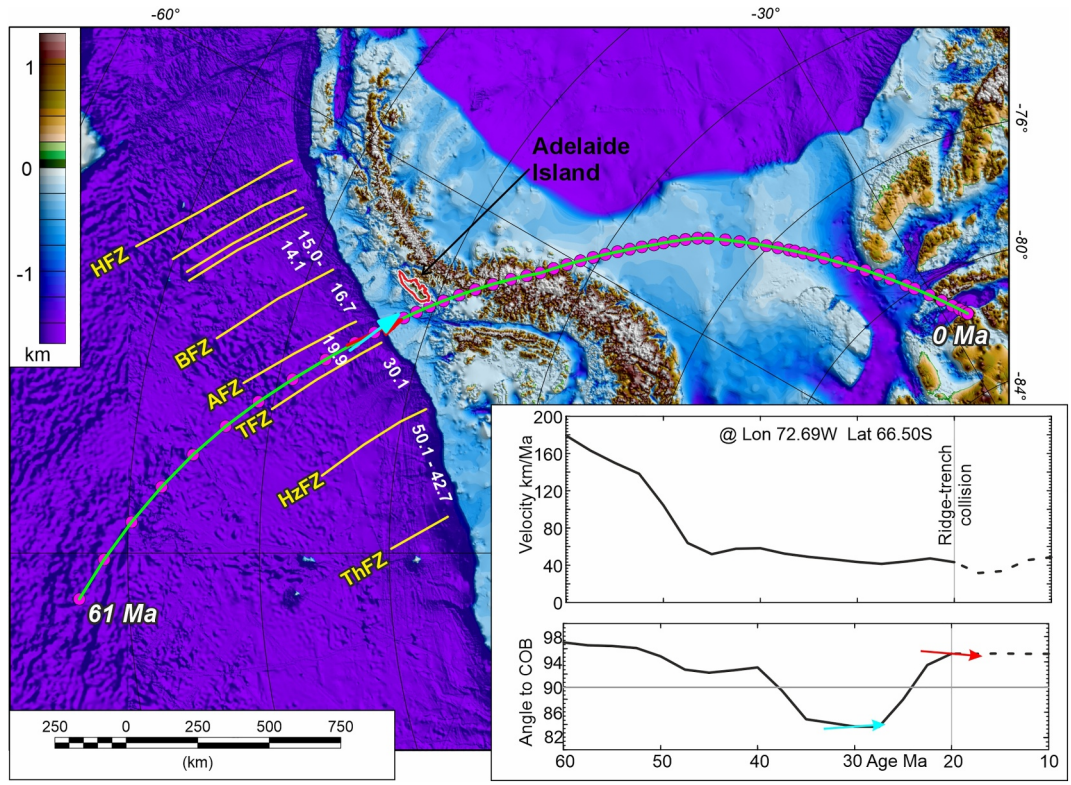

Figure 8. Example Phoenix plate flow-line (green line) tracking a particle from 61 to 0 Ma from the rotation model of Burton-Johnson et al. (2023), implemented in GPlates (Müller et al., 2018). Pink dots mark particle location at 1 Ma intervals. Arrows show subduction direction directly adjacent to the study area at 30 Ma (blue) and 20 Ma (red). Fracture Zones as yellow lines include Tharp (ThFZ), Heezen (HzFZ), Tula (TFZ), Adelaide (AFZ), Bisco (BFZ) and Hero (HFZ) (Larter et al., 1997). Small white numbers show age of ridge-trench collision (Larter et al., 1997). Inset profiles show convergence rate and angle relative to the Continent Ocean Boundary (COB), outboard from southern Adelaide Island. Note velocity and angle calculated for distinct flow lines, each intersecting the COB at 2.5 Ma increments.

fabric pre-dated or was coincident with the main ~50 Ma phase of magmatism, correlation with the magnetic trends might be expected. We therefore interpret this fabric as a younger feature. Thermal history modeling suggests a rapid ~20 Ma cooling (uplift and denudation) event on the Faure Islands (Karaoğlan et al., 2023). This age approximately coincides with ~23 Ma magmatism to the north on the eastern edge of Adelaide Island, which, in contrast to the intrusions within Marguerite Bay, shows a well-defined NNE trend (Jordan et al., 2014), corresponding closely with the trend in the GoPro imagery. This correspondence leads us to suggest that a major tectonic event occurred ~20 Ma driving deformation parallel to the subduction zone, but with magmatism restricted to the north. It has been proposed that subduction against the northern Antarctic Peninsula margin (~62°S) was highly oblique through the Cenozoic (Eagles & Scott, 2014), which could favor strike-slip deformation parallel to the trench. However, analysis of recent reconstructions (Burton-Johnson et al., 2023) focusing specifically on the region of Marguerite Bay (~66.5°S), show that convergence was approximately orthogonal until collision (Figure 8). An alternative mechanism for driving trench parallel deformation must therefore be sought. We propose that cessation of subduction at ~20 Ma between the Tula and Adelaide fracture zones immediately out-board of Marguerite Bay was the key driver of deformation. This event may have triggered more intense local toroidal mantle flow around the newly developed slab edge (Schellart, 2024). Such flow would be trench parallel, exerting basal shear stress on the overlying crust and creating trench parallel deformation within the upper crust. The impact of trench parallel flow on deformation has not been robustly considered, with most previous studies of subduction systems focusing on compressional or extensional end-members (Schellart, 2024). Toroidal-mode mantle flows associated with subduction of broken plates have been seismically imaged and theoretically modeled in the mantle in Central America (Zhu et al., 2020). However, we propose that the Marguerite Bay region of Antarctica may hold critical evidence of this process impacting upper crustal deformation and magmatism.

5. Conclusions

Joint inversion of new high-resolution gravity and magnetic data reveal the size, shape and composition of igneous intrusions in the Marguerite Bay region of the Antarctic Peninsula. Two main intrusions of granodioritic composition are identified, which have a combined volume of ~7,400 km^3, forming ~20% of the crustal volume in the study area. Additionally, minor granitic intrusions and a likely thick sequence of sedimentary rocks are also interpreted in the study region.

The absence of any structural control on the main granodiorite intrusions points to their emplacement independent of crustal deformation associated with the onshore continuation of oceanic fracture zones, although we cannot rule out a role for such structures in the subducted plate controlling the locus of magma generation. The interpreted intrusions were most likely emplaced at ~50 Ma, ~30 Ma before the local cessation of subduction. However, they are temporally associated with slowing subduction and ridge-trench collision to the south, which likely facilitated regional extension, focusing of magmatism and a shift in magma locus toward the continental margin.

There is evidence from aerial imagery of a major structural event running parallel to the Peninsula margin, which we attribute to deformation associated with enhanced toroidal trench parallel mantle flow created as subduction shut down at ~20 Ma. This event was generally a-magmatic in Marguerite Bay where subduction ceased, but likely contributed to structurally controlled magmatism further north on the Antarctic Peninsula.

We propose that the spatial and temporal pattern of magmatism and deformation point to the importance of teleconnection in the magmatic system along the subduction system, as well as across it, likely driven by changes in mantle flow. This hypothesis requires verification with more detailed understanding of the relative ages and pattern of structural control of magmatism along the Antarctic Peninsula.

Data Availability Statement

Airborne geophysical data including magnetic (Jordan, Lowe, et al., 2024) and gravity (Jordan, Robinson, et al., 2024) information collected by this project, together with the inversion output (Lowe & Jordan, 2024) are available from the NERC UK Polar Data Centre. Python notebooks required to run the jif3d inversion (Moorkamp et al., 2023) are available from Zenodo (Lowe, 2024). Other data sets and code referenced in the text are available from the sources cited. Unless otherwise stated in the text geophysical data processing and visualization was carried out in the commercially available Geosoft package, available from Seequent Ltd. https://www.seequent.com/.

Acknowledgments
Data collection and processing was funded by UKRI Innovate UK through their Future flight challenge support for the "Protecting environments with unmanned aerial vehicle swarms" project (reference: 10023377). We also thank staff from Windracers Ltd, the BAS operations and engineering team, and BAS air unit whose hard work and dedication made this project possible, and thank the editor and two reviewers who helped us refine and improve our manuscript.

References

Burton-Johnson, A., Bastias, J., & Kraus, S. (2023). Breaking the ring of fire: How ridge collision, slab age, and convergence rate narrowed and terminated the Antarctic Continental Arc. *Tectonics*, *42*(5), e2022TC007634. https://doi.org/10.1029/2022TC007634

Canny, J. (1986). A computational approach to edge detection. *IEEE Transactions on Pattern Analysis and Machine Intelligence*, *8*(6), 679–698. https://doi.org/10.1109/tpami.1986.4767851

Cooper, G. R. J., & Cowan, D. R. (2006). Enhancing potential field data using filters based on the local phase. *Computers & Geosciences*, *32*(10), 1585–1591. https://doi.org/10.1016/j.cageo.2006.02.016

Dorschel, B., Hehemann, L., Viquerat, S., Warnke, F., Dreutter, S., Tenberge, Y. A., et al. (2022). The international bathymetric chart of the Southern Ocean version 2 (IBCSO v2). https://doi.org/10.1594/PANGAEA.937574

Eagles, G., Gohl, K., & Larter, R. D. (2009). Animated tectonic reconstruction of the Southern Pacific and alkaline volcanism at its convergent margins since Eocene times. *Tectonophysics*, *464*(1–4), 21–29. https://doi.org/10.1016/j.tecto.2007.10.005

Eagles, G., & Scott, B. G. C. (2014). Plate convergence west of Patagonia and the Antarctic Peninsula since 61 Ma. *Global and Planetary Change*, *123*, 189–198. https://doi.org/10.1016/j.gloplacha.2014.08.002

Golynsky, A. V., Ferraccioli, F., Hong, J. K., Golynsky, D. A., Frese, R. R. B., Young, D. A., et al. (2018). New magnetic anomaly map of the Antarctic. *Geophysical Research Letters*, *45*(13), 6437–6449. https://doi.org/10.1029/2018gl078153

Johnson, A. (1997). Cenozoic tectonic evolution of the Marguerite Bay area, Antarctic Peninsula, interpreted from geophysical data. *Antarctic Science*, *9*(3), 268–280. https://doi.org/10.1017/s0954102097000369

Johnson, A. (1999). Interpretation of new aeromagnetic anomaly data from the central Antarctic Peninsula. *Journal of Geophysical Research*, *104*(B3), 5031–5046. https://doi.org/10.1029/1998jb900073

Johnson, A., & Swain, C. J. (1995). Further evidence of fracture-zone induced tectonic segmentation of the Antarctic Peninsula from detailed aeromagnetic anomalies. *Geophysical Research Letters*, *22*(14), 1917–1920. https://doi.org/10.1029/95gl00812

Jordan, T., Lowe, M., Robinson, C., Reed, T., & Toomey, R. (2024). Processed aeromagnetic line data flown from Rothera station with a Windracers Ultra UAV (2023/24 season) (Version 1.0) [Dataset]. *NERC EDS UK Polar Data Centre*. https://doi.org/10.5285/4bcc9b4e-fab5-46cd-aac3-56c28e61cff1

Jordan, T., Robinson, C., Reed, T., & Toomey, R. (2024). Airborne gravity data over Marguerite Bay collected with a Windracers Ultra UAV (2023/24 season) (Version 1.0) [Dataset]. *NERC EDS UK Polar Data Centre*. https://doi.org/10.5285/3a9c8604-2bca-48c1-a40c-48a873076581

Jordan, T. A., & Becker, D. (2018). Investigating the distribution of magmatism at the onset of Gondwana breakup with novel strapdown gravity and aeromagnetic data. *Physics of the Earth and Planetary Interiors*, *282*, 77–88. https://doi.org/10.1016/j.pepi.2018.07.007

Jordan, T. A., Neale, R. F., Leat, P. T., Vaughan, A. P. M., Flowerdew, M. J., Riley, T. R., et al. (2014). Structure and evolution of Cenozoic arc magmatism on the Antarctic Peninsula: A high resolution aeromagnetic perspective. *Geophysical Journal International*, *198*(3), 1758–1774. https://doi.org/10.1093/gji/ggu233

Jordan, T. A., Robinson, C., Reed, T., Toomey, R., Jelev, N., Waters, J., et al. (2025). Successful deployment of a large UAV for multi-disciplinary science from Rothera Research Station Antarctica; 2024 season overview and lessons learned. *Antarctic Science*, 1–18. https://doi.org/10.1017/S0954102025000136

Karaoğlan, F., KarataŞ, B., Özdemir, Y., Gülyüz, E., Vassilev, O., Selbesoğlu, M. O., & Gildir, S. (2023). The geo/thermochronology of Dismal Island (Marguerite Bay, Antarctic Peninsula). *Turkish Journal of Earth Sciences*, *32*(8), 975–988. https://doi.org/10.55730/1300-0985.1887

Larter, R. D., & Barker, P. F. (1991). Effects of ridge crest-trench interaction on Antarctic-Phoenix spreading: Forces on a young subducting plate. *Journal of Geophysical Research*, *96*(B12), 19583–19607. https://doi.org/10.1029/91jb02053

Larter, R. D., Rebesco, M., Vanneste, L. E., Gambôa, L. A. P., & Barker, P. F. (1997). Cenozoic tectonic, sedimentary and glacial history of the continental shelf west of Graham Land, Antarctic Peninsula. *Antarctic Research Series*, *71*, 1–27. https://doi.org/10.1029/ar071p0001

Leat, P. T., Flowerdew, M. J., Riley, T. R., Whitehouse, M. J., Scarrow, J. H., & Millar, I. L. (2009). Zircon U-Pb dating of Mesozoic volcanic and tectonic events in north-west Palmer Land and south-west Graham Land, Antarctica *Antarctic Science*. *Antarctic Science*, *21*(6), 633–641. https://doi.org/10.1017/s0954102009990320

Lösing, M., Moorkamp, M., & Ebbing, J. (2023). Joint inversion based on variation of information—A crustal model of Wilkes Land, East Antarctica. *Geophysical Journal International*, *232*(1), 162–175. https://doi.org/10.1093/gji/ggac334

Lowe, M. (2024). MaximilianLowe/VI_inversion_SWARM: SWARM_VI_inversion (Version v1) [software]. *Zenodo*. https://doi.org/10.5281/zenodo.14016296

Lowe, M., Jordan, T., Ebbing, J., Koglin, N., Ruppel, A., Moorkamp, M., et al. (2024). Comparing geophysical inversion and petrophysical measurements for northern Victoria Land, Antarctica. *Geophysical Journal International*, *239*(1), 276–291. https://doi.org/10.1093/gji/ggae272

Lowe, M., Jordan, T., Moorkamp, M., Ebbing, J., Green, C., Lösing, M., et al. (2024). The 3D crustal structure of the wilkes subglacial Basin, East Antarctica, using variation of information joint inversion of gravity and magnetic data. *Journal of Geophysical Research: Solid Earth*, *129*(10), e2023JB027794. https://doi.org/10.1029/2023JB027794

Lowe, M., & Jordan, T. A. (2024). 3D density and susceptibility distribution model derived from 2024 gravity and magnetic surveys of Marguerite Bay, West Antarctica (Version 1.0) [Dataset]. *NERC EDS UK Polar Data Centre*. https://doi.org/10.5285/4c8cfe1b-f426-4cc7-819b-236d1058ea0d

Magni, V., Bouilhol, P., & van Hunen, J. (2014). Deep water recycling through time. *Geochemistry, Geophysics, Geosystems*, *15*(11), 4203–4216. https://doi.org/10.1002/2014GC005525

McCarron, J. J., & Millar, I. L. (1997). The age and stratigraphy of fore-arc magmatism on Alexander Island, Antarctica. *Geological Magazine*, *134*(4), 507–522. https://doi.org/10.1017/s0016756897007437

Millar, I. L., Pankhurst, R. J., & Fanning, C. M. (2002). Basement chronology of the Antarctic Peninsula: Recurrent magmatism and anatexis in the Palaeozoic Gondwana Margin. *Journal of the Geological Society*, *159*(2), 145–157. https://doi.org/10.1144/0016-764901-020

Millar, I. L., Willan, R. C. R., Wareham, C. D., & Boyce, A. J. (2001). The role of crust and mantle sources in the genisis of granitoids of the Antarctic Peninsula and adjacent crustal blocks. *Journal of the Geological Society London*, *158*(5), 855–867. https://doi.org/10.1144/0016-764900-139

Moorkamp, M. (2021). Joint inversion of gravity and magnetotelluric data from the Ernest-Henry IOCG deposit with a variation of information constraint. In *First international meeting for applied geoscience & energy expanded abstracts* (pp. 1711–1715). Society of Exploration Geophysicists.

Moorkamp, M., Heincke, B., Jegen, M., Roberts, A. W., & Hobbs, R. W. (2011). A framework for 3-D joint inversion of MT, gravity and seismic refraction data. *Geophysical Journal International*, *184*(1), 477–493. https://doi.org/10.1111/j.1365-246X.2010.04856.x

Moorkamp, M., Heincke, B., Shi, Z., & Weise, B. (2023). Joint inversion framework in three dimensions (JIF3D) [Software]. https://sourceforge.net/projects/jif3d/

Morlighem, M., Rignot, E., Binder, T., Blankenship, D., Drews, R., Eagles, G., et al. (2020). Deep glacial troughs and stabilizing ridges unveiled beneath the margins of the Antarctic ice sheet. *Nature Geoscience*, *13*(2), 132–137. https://doi.org/10.1038/s41561-019-0510-8

Müller, R. D., Cannon, J., Qin, X., Watson, R. J., Gurnis, M., Williams, S., et al. (2018). GPlates: Building a virtual Earth through deep time. *Geochemistry, Geophysics, Geosystems*, *19*(7), 2243–2261. https://doi.org/10.1029/2018gc007584

Pappa, F., Ebbing, J., & Ferraccioli, F. (2019). Moho depths of Antarctica: Comparison of seismic, gravity, and isostatic results. *Geochemistry, Geophysics, Geosystems*, *20*(3), 1629–1645. https://doi.org/10.1029/2018gc008111

Riley, T. R., Burton-Johnson, A., Flowerdew, M. J., & Whitehouse, M. J. (2018). Episodicity within a mid-Cretaceous magmatic flare-up in West Antarctica: U-Pb ages of the Lassiter Coast intrusive suite, Antarctic Peninsula, and correlations along the Gondwana margin. *GSA Bulletin*, *130*(7–8), 1177–1196. https://doi.org/10.1130/B31800.1

Riley, T. R., Flowerdew, M. J., Carter, A., Curtis, M. L., Millar, I. L., Crame, J. A., & Whitehouse, M. J. (2024). Tracking the tempo of a continental margin arc: Insights from a forearc succession in West Antarctica. *GSA Bulletin*, *136*(11–12), 5039–5057. https://doi.org/10.1130/B37558.1

Riley, T. R., Flowerdew, M. J., & Haselwimmer, C. E. (2011). Geological Map of Adelaide Island, Graham Land (1:200000 scale).

Riley, T. R., Flowerdew, M. J., & Whitehouse, M. J. (2012a). Chrono- and lithostratigraphy of a Mesozoic–Tertiary fore-to intra-arc basin: Adelaide Island, Antarctic Peninsula. *Geological Magazine*, *149*(5), 768–782. https://doi.org/10.1017/S0016756811001002

Riley, T. R., Flowerdew, M. J., & Whitehouse, M. J. (2012b). U–Pb ion-microprobe zircon geochronology from the basement inliers of eastern Graham Land, Antarctic Peninsula. *Journal of the Geological Society*, *169*(4), 381–393. https://doi.org/10.1144/0016-76492011-142

Riley, T. R., & Leat, P. T. (1999). Large volume silicic volcanism along the proto-Pacific margin of Gondwana: Lithological and stratigraphical investigations from the Antarctic Peninsula. *Geological Magazine*, *136*, 1–16. https://doi.org/10.1017/s0016756899002265

Salem, A., Williams, S., Fairhead, J. D., Ravat, D., & Smith, R. (2007). Tilt-depth method: A simple depth estimation method using first-order magnetic derivatives. *The Leading Edge*, *26*(12), 1502–1505. https://doi.org/10.1190/1.2821934

Sanchez, G., Halpin, J. A., Gard, M., Hasterok, D., Stål, T., Raimondo, T., et al. (2021). PetroChron Antarctica: A geological database for interdisciplinary use. *Geochemistry, Geophysics, Geosystems*, *22*(12), e2021GC010154. https://doi.org/10.1029/2021GC010154

Schellart, W. P. (2024). Subduction dynamics and overriding plate deformation. *Earth-Science Reviews*, *253*, 104755. https://doi.org/10.1016/j.earscirev.2024.104755

Twinn, G., Riley, T., Fox, M., & Carter, A. (2022). Thermal history of the southern Antarctic Peninsula during Cenozoic oblique subduction. *Journal of the Geological Society*, *179*(6). https://doi.org/10.1144/jgs2022-008

Vaughan, A. P. M., Eagles, G., & Flowerdew, M. J. (2012). Evidence for a two-phase Palmer Land Event from cross-cutting structural relationships and emplacement timing of the Lassiter Coast Intrusive Suite, Antarctic Peninsula: Implications for mid-Cretaceous Southern Ocean plate configuration. *Tectonics*, *31*(1), TC1010. https://doi.org/10.1029/2011TC003006

von Frese, R. R. B., Hinze, W. J., Braile, L. W., & Luca, A. J. (1981). Spherical earth gravity and magnetic anomaly modeling by Gauss- Legendre quadrature integration. *Journal of Geophysics*, *49*, 234–242.

Wendt, A. S., Vaughan, A. P. M., Ferraccioli, F., & Grunow, A. M. (2013). Magnetic susceptibilities of rocks of the Antarctic Peninsula: Implications for the redox state of the batholith and the extent of metamorphic zones. *Tectonophysics*, *585*, 48–67. https://doi.org/10.1016/j.tecto.2012.07.011

Wessel, P., Smith, W. H. F., Scharroo, R., Luis, J., & Wobbe, F. (2013). Generic mapping tools: Improved version released. *Eos, Transactions American Geophysical Union*, *94*(45), 409–410. https://doi.org/10.1002/2013EO450001

Zhu, H., Stern, R. J., & Yang, J. (2020). Seismic evidence for subduction-induced mantle flows underneath Middle America. *Nature Communications*, *11*(1), 2075. https://doi.org/10.1038/s41467-020-15492-6